Investigation on Aerodynamic Performance of Elliptical and Secant give Nose Cones

Danish Parvez   Sonia Chalia
Department of Aerospace Engineering
Amity University Gurugram, India
Danishparvez003@gmail.com

Abstract-In this paper, the computational and experimental approach was used to study the aerodynamic performance of elliptical and secant ogive nose cone profiles. The aerodynamic characteristic's such as pressure, coefficient of pressure, axial velocity, total drag, dynamic pressure etc. for the secant and elliptical nose cone profiles were illustrated for low subsonic speeds for the same length to diameter ratio. Simulation were carried out with inlet velocity of 25 m/s, calculated for zero angle of attack to demonstrate the flow behaviour around the nose cone profiles. The data obtained from the computational analysis of the nose cone shapes was compared with the experimental data obtained from the wind tunnel analysis in order to find out the deviation. It was found out that the elliptical nose cone experienced less skin friction drag in comparison to secant ogive. Also, the velocity near the trailing edge in case of secant ogive was found out to be more when compared to elliptical nose cone. After comparing both the nose cones on the basis of coefficient of drag, skin friction drag and total drag experienced by the body, elliptical nose cone was found to be most efficient amongst the two.

Keyword-Secant ogive, Elliptical nose cone, Static pressure, Coefficient of pressure, Drag, Computational Fluid Dynamics CFD, Velocity, Coefficient of drag.

NOMENCLATURE
D Diameter of nose cone at body tube joint
L   Length of nose cone
X   Distance along nose cone measured from body tube joint
Y   Radius
P   Power or parameter used to specify haack sub type

I. INTRODUCTION

External flows past objects leads to a variety of fluid mechanics phenomena. Primarily the character of the flow field depends on the profile of the object as such that, even the simplest shaped objects for e.g. a sphere, produces a rather complex flow. Various parameters such as size, orientation, speed and fluid properties define the flow pattern and related forces over a body. Proper understanding of the flow features around the nose is extremely important due to the placement of payload.

Payload is usually placed around the nose cone in slender bodies such as launch vehicles, rockets, missiles etc. If we consider the geometry of the main rocket engines as well as the volume of the payload along with the specific requirements of a mission, use of conical nose cone shapes along with boat tail are of extreme importance [1]. The following parameters govern the nose cone geometry as illustrated in figure 1.**"The Descriptive Geometry of Nose Cone," 1996***)*
1.Types of Nose Cone - The selection of a particular type of nose cone depends upon the speed and the mission of the vehicle. As such there are a number of different nose cone profiles such as Secant ogive, Tangent ogive, Elliptical, Conical, Bi-conic, Parabolic, Power series, Haack series. Given below are the nose cones of interest:

Table 1 Parameters governing nose cone geometry

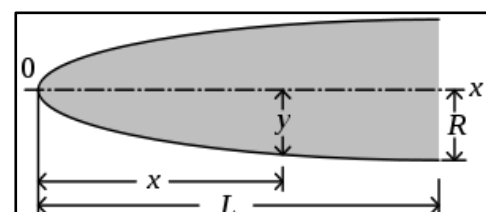|	
L	Overall length
R	Radius of the base
y	Radius at any point x, also x varies from 0 to L
C/L	The full body of revolution of the nosecone is formed by rotating the profile around the centreline

Figure 1 Nose cone Nomenclature (Source G. A. C. Sr.,)

2. Secant Ogive Nose Cone

The profile of this shape is formed by a segment of a circle as shown in figure 2, but the base of the shape is not on the radius of the circle defined by the ogive radius (ρ). In this case the rocket body will not be tangent to the curve of the nose at its base. Therefore, the ogive radius $\rho$is not determined by R and L, but is one of the factors to be chosen to define the nose shape. The radius Y at any point x as x varies from 0 to L is given by equation 1 [2].

$$Y = \frac{D}{2} * \left[1 - \left(\frac{X+F}{A}\right)^p\right] * \left[\frac{A^p}{A^P - F^P}\right] \qquad (1)$$

If $0 < F < L$, then result is secant ogive type [2]
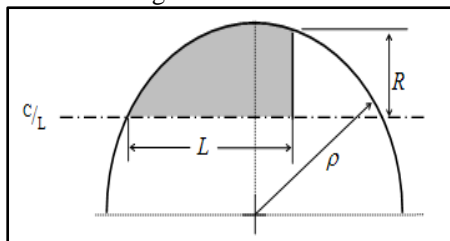(True secant ogive has P=2)
Also, F=3 for secant ogive

Figure 2 Secant ogive Nose cone (Source:G. A. C. Sr., "The Descriptive Geometry of Nose Cone," 1996)

3.Elliptical Ogive Nose Cone

This shape is one-half of an ellipse, with the major axis being the Centre line (C/L) and the minor axis being the base of the nose cone as shown in figure 3. This shape is efficient for subsonic flight conditions due to its blunt nose and tangent base [3].The radius Y at any point x as x varies from 0 to L is given by equation 2.

$$Y = \left[\left(\frac{D}{2}\right)^p * \left[1 - \left(\frac{X}{L}\right)^P\right]\right]^{\frac{1}{P}} \qquad (2)$$
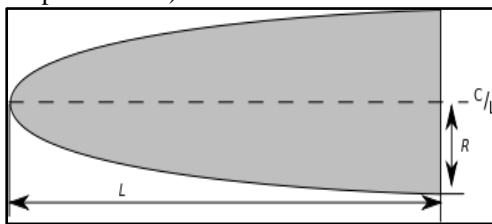
(True ellipse has P=2)

Figure 3Elliptical Nose cone (Source:G. A. C. Sr., "The Descriptive Geometry of Nose Cone," 1996)

II. LITERATURE REVIEW

1.Historical Background Of Nose Cone Design

Nose cone geometry has been a topic discussed for more than a century. The geometry of a nose cone is critical to an object's aerodynamic characteristics. Yefremov and Takovitskii used the Euler equations to design nose cone designs with specified dimensions and volumes leading to minimal aerodynamic wave drag. Foster and

Dulikravich used two methods in order to compare and differentiate their performance on optimization of nose shape geometry [4].Furthermore, taking into account the aerodynamic drag, heat transfer, and payload volume, Lee et al. obtained an optimal nose cone shape through the use of a multipoint response surface design method[5].

2. Effect of Different Nose Cone Profiles On Subsonic Pressure Coefficients

The nose shape does not affect the cross-flow pressure distribution at all, however part of the adverse pressure gradient that is generated from the longitudinal flow can be changed by altering the nose shape [6].A system of procedures was employed by Munk for analysis in order to find the minimum Cp and critical Mach number. Using Munk Airship Theory the nose dimensions were first sent through an incompressible Cp calculation from which, a distribution of incompressible pressure coefficients was formed. After that the minimum pressure coefficient that was calculated in the first step was chosen to run through an incompressible to compressible transformation known as the Karman-Tsien Correction, which is valid for subsonic Mach numbers [7].

III. NUMERICAL METHODOLOGY

1. Governing Equations

The two-dimensional (2D) steady axisymmetric governing equations, which govern the occurrence of the physical phenomena when there is a flow past nose cone are as follows [8]:

$$\frac{\partial}{\partial x}(\rho u_x) + \frac{1}{r}\frac{\partial}{\partial r}(r\rho u_r) = 0 \qquad (3)$$

Where x is the axial coordinate, r is the radial coordinate, where $u_x$is the axial velocity, and $u_r$is the radial velocity.
Momentum conservation equation (axial direction):

$$\frac{1}{r}\frac{\partial}{\partial x}(r\rho u_x u_x) + \frac{1}{r}\frac{\partial}{\partial r}(r\rho u_r u_x)$$
$$= -\frac{\partial p}{\partial x}$$
$$+ \frac{1}{r}\frac{\partial}{\partial x}\left[r\mu\left(2\frac{\partial u_x}{\partial x}\right.\right.$$
$$\left.\left.- \frac{2}{3}\left(\nabla \cdot \vec{u}\right)\right)\right]$$
$$+ \frac{1}{r}\frac{\partial}{\partial x}\left[r\mu\left(\frac{\partial u_x}{\partial r} + \frac{\partial u_r}{\partial x}\right)\right]$$
$$+ F_x$$

(4)

Momentum conservation equation (radial direction):

$$\frac{1}{r}\frac{\partial}{\partial x}(r\rho u_x u_r) + \frac{1}{r}\frac{\partial}{\partial r}(r\rho u_r u_r) \quad (5)$$

$$= -\frac{\partial p}{\partial r}$$

$$+ \frac{1}{r}\frac{\partial}{\partial x}\left[r\mu\left(\frac{\partial u_r}{\partial x} + \frac{\partial u_x}{\partial r}\right)\right]$$

$$+ \frac{1}{r}\frac{\partial}{\partial r}\left[r\mu\left(2\frac{\partial u_r}{\partial r}\right.\right.$$

$$\left.\left. - \frac{2}{3}\left(\nabla.\vec{u}\right)\right)\right] - 2\mu\frac{u_r}{r^2}$$

$$+ \frac{2}{3}\frac{\mu}{r}(\nabla.\vec{u}) + \rho\frac{u_z^2}{r} + F_r$$

$$\nabla.\vec{u} = \frac{\partial u_x}{\partial x} + \frac{\partial u_r}{\partial r} + \frac{u_r}{r} \quad (6)$$

F_x and F_r comprise external body forces, model-dependent source terms, and user-defined sources, and u_z is the swirl velocity.

2. Energy conservation equation:

$$\nabla.\left(\vec{u}(\rho E + p)\right) = \nabla.\left(k_{eff}\nabla T + \left(\overline{\overline{\tau_{eff}}} . \vec{u}\right)\right) \quad (7)$$

Where k_{eff} is the effective thermal conductivity ($k_{eff}=k+k_t$) and k_t is the turbulent thermal conductivity defined based on turbulence model. The first term on the right-hand side of energy conservation equation represents energy transfer due to conduction, which is zero due to adiabatic boundary conditions imposed on the nose cone surface, and the second term represents viscous dissipation.

3.Equation of state:

$$p = \rho R_c T \quad (8)$$

4.Solution Method
Numerical solution was obtained using ANSYS CFD which includes the provision for geometry design, grid generation, flow simulations, and analysis of results. Since, the nose cone as well as created computational domain was principally symmetric about the axis, only upper half would essentially have the similar flow. The computational domain was an arc with radius 585mm for predicting the various aerodynamic parameters. Also Transition SST model was used along with inviscid model to carry out the simulation.

5.Geometry and Domain
The following geometries were analyzed in the ANSYS as shown in figure 4.
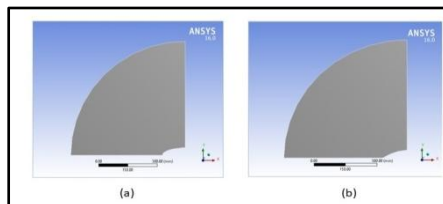

Figure 4 Geometry (a) ellipse; (b) secant ogive.

Table 2Domain parameters

Radius of domain (mm)	Length of the model (mm)	Base diameter of the model(mm)
585	117	78

6. Grid Independency Test
To ensure that the aerodynamic parameters were independent of the number of cells in the constructed grid, a grid independency test was performed. Structured grids with strictly quadrilateral cells were constructed with varying divisions i.e. 200, 225, 250, 275, 300, 325 and 300 nodes on each edge of the domain as shown in figure 6. Coefficient of drag encountered by a conical nose cone having finesse ratio 3 was considered and compared to perform the grid independency test as shown in figure 7. The name selection of the domain is given in Figure 5.
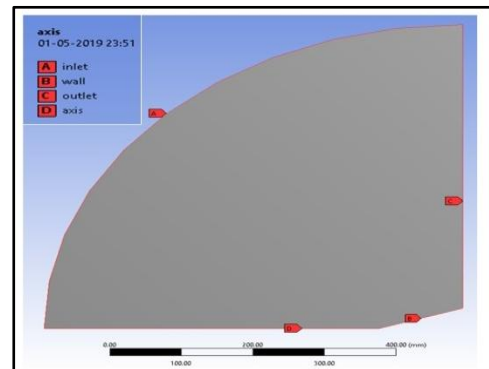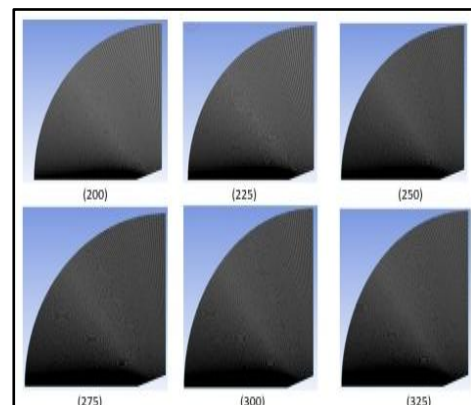

Figure 5 Name selection.
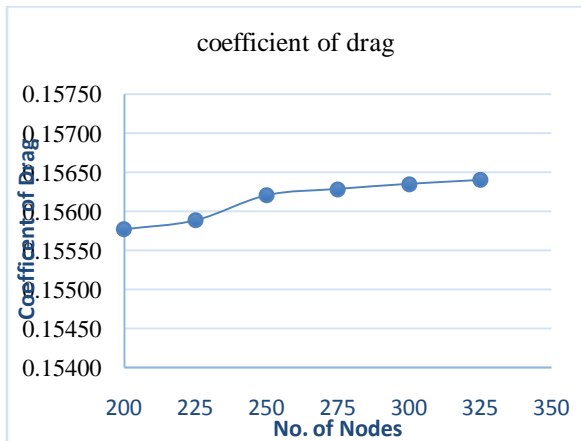

Figure 6 Different mesh sizes.

Figure 7 Grid independency graph.

7. Meshing

Mesh generation is the practice of generating a polygonal mesh that approximates a geometric domain as shown in figure 8. The term "grid generation" is often used interchangeably. The mesh influences the accuracy, convergence and computation time and hence is one of the most important steps in computation analysis [9].
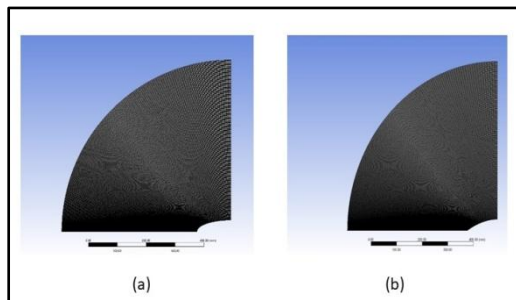

Figure 8 Meshing (a)ellipse; (b)secant ogive.

Table 3 Mesh control

Object Name	Edge Sizing	Edge Sizing 2	Face Meshing
State	Fully Defined		
Scope			
Scoping Method	Geometry Selection		
Geometry	2 Edges		1 Face
Definition			
Suppressed	No		
Type	Number of Divisions		
Number of Divisions	275	300	
Behaviour	Hard		
Bias Type	--------------	No Bias	
Bias	20.		

Factor			
Reverse Bias	1 Edge		
Mapped Mesh			Yes
Method			Quadrilaterals
Constrain Boundary			No
Advanced			
Specified Sides			No Selection
Specified Corners			No Selection
Specified Ends			No Selection

8.Turbulence Models

Fluctuating velocity fields are used to characterize Turbulent flows. During turbulent flow quantities such as momentum, energy, and species concentration, are mixed as a result of these fluctuations due to which the transported quantities fluctuate too. Due to their small scale and high frequency these fluctuations are computationally expensive, to simulate directly in practical engineering calculations [10]. Therefore, in order to remove the resolution of small scales, a modified set of equations that are computationally less expensive to solve are established in place of the instantaneous governing equations. These modified equations contain additional variables whose values are unknown. As a result, turbulence models are required to find these unknown variables in terms of already known quantities. [11]

9.Boundary Conditions

A double precision, implicit, pressure based solver was utilized to perform steady, inviscid, axial simulations to predict the body/airflow interaction and behaviour of various aerodynamic phenomena for airflow past secant ogive and elliptical nose cone. The incoming fluid was considered to be air with a velocity of 25 m/s calculated at zero degrees angle of attack. The simulation was carried on the above mentioned nose cones using K-ω SST turbulence model.Themodel was chosen for numerical analysis as this model is best suitable for flows transitioning from laminar to turbulent along with being computationally less expensive. This model also includes the skin friction drag and has a lesser sensitivity towards numerical error [12].

IV. PROBLEM SPECIFICATION

A computational and experimental approach is used to study the aerodynamic performance of elliptical and secant ogive nose cone profiles. The data obtained from the computational analysis of the nose cone profiles is then compared with the experimental data obtained from the wind tunnel analysis in order to find out the variation

between them. The simulation involves the velocity of 25 m/s calculated at zero degrees angle of attack in order to demonstrate the flow behavior around various nose cone profiles.

V. VALIDATION OF EXPERIMENTAL SETUP

In order to validate experimental setup to conduct experimental analysis, Coefficient of Pressure (Cp) was calculated for a cylinder with dimensions (300mm x 50 mm) was found out at various angles and then compared with theoretical data as shown in figure 9. Furthermore, wind tunnel calibration was also carried out in order to determine inlet velocity
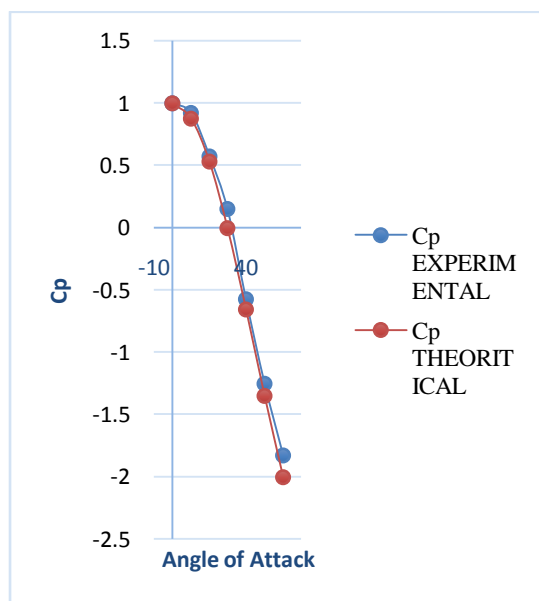

Figure 9Comparison between Cp theoretical and Cp experimental.

VI. RESULTS AND DISCUSSIONS

1. Computational Results

Parameters such as velocity, static pressure, and dynamic pressure were obtained from the ANSYS fluent.

2. Variation In Static And Dynamic Pressure Along The Curve Length

2.1 Secant ogive

Figures 10 and 11 show the variation in dynamic and static pressure along the curve length from the tip of the profile and contours respectively.it can be observed that static pressure at the tip of the nose cone is maximum and starts decreasing gradually along the curve length whereas the value of dynamic pressure is minimum on the tip and starts increasing gradually along the curve length. All these changes can be verified by the static and dynamic contours of the Secant ogive profile as shown in figure 11.
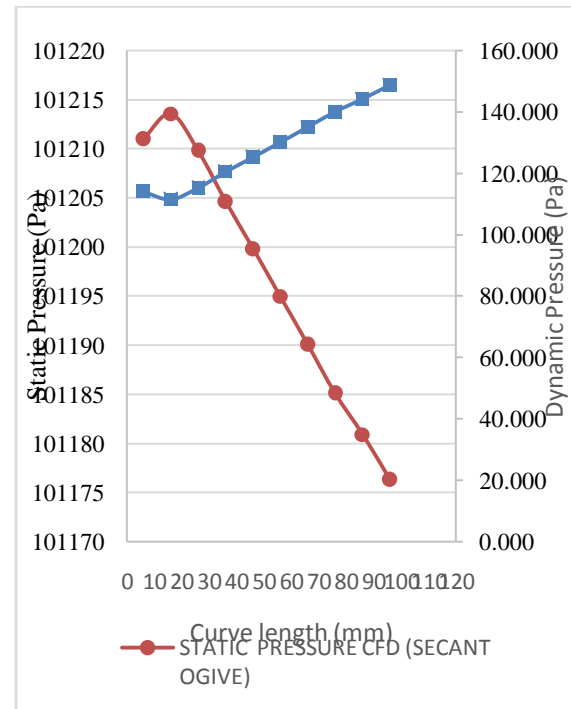

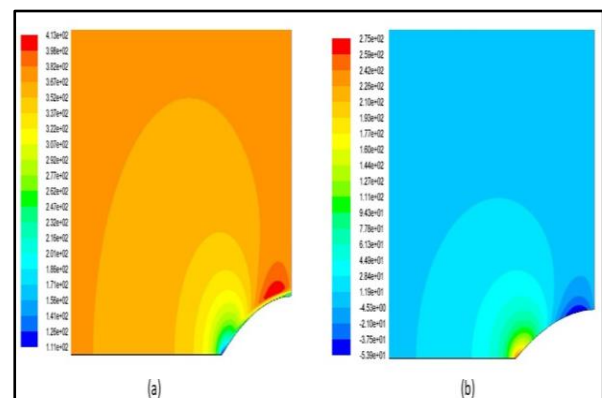Figure 10Dynamic and static pressure variation on secant ogive

Figure 11(a)Dynamic pressure contour for Secant ogive; (b) Static pressure contour for Secant ogive

2.2 Ellipse nose cone

The Figures 12 and 13 show the variation in dynamic and static pressure along the curve length from the tip of the profile. It can be observed that static pressure at the tip of the nose cone is maximum and starts decreasing drastically along the curve length when compared to the secant ogive. Also the value of dynamic pressure is minimum on the tip and starts increasing drastically along the curve length when compared to that of secant ogive. All these changes can be verified by the static and dynamic contours of the Secant ogive profile.
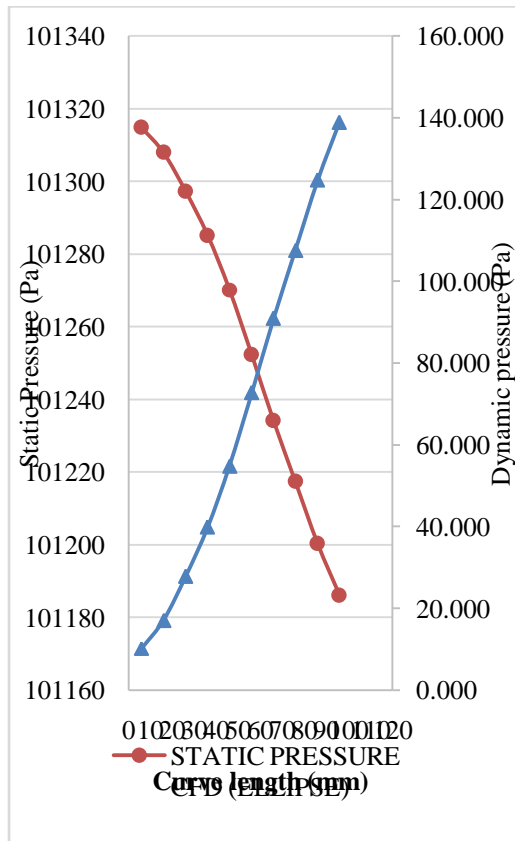
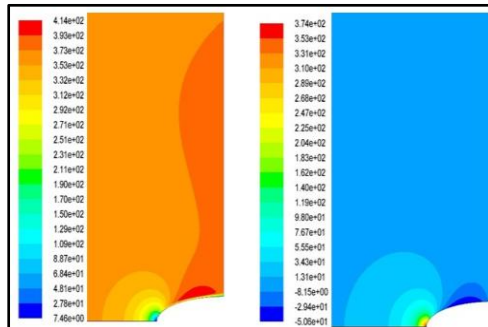Figure 12Dynamic and Static pressure variation on ellipse nose cone

Figure 13(a) Dynamic pressure contour for ellipse nose cone; (b) Static pressure contour for ellipse nose cone

2.3 Variation in Velocity along The Cur5ve Length
Figure 14shows the variation of velocity along the curve length of both the secant ogive and elliptical nose cone profile respectively. As seen in the figure the variation in velocity is more in case of elliptical nose cone profile due to the generation of stagnation point at the tip of the profile caused due to the blunt shape of the profile whereas the variation in velocity in case of secant ogive is minimal due to the blunt nature of its shape.
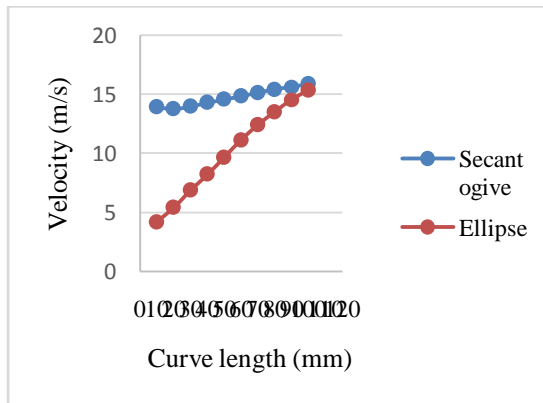
Figure 14Velocity graph for different nose cone profiles

2.4 Streamline and Vector Contours
The streamlines are used to check the behaviour of the flow while the vector controls are used to know the existence of the vortex on the surface of the profile. Figure 15 and 16 represent the streamline and vector contours over secant and elliptical nose cone profiles respectively.

2.4.1Secant ogive

Figure 15(a) Streamline over secant ogive; (b) Velocity vector over secant ogive

2.4.2 Ellipse nose cone

Figure 16(a) Streamline over elliptical nose cone; (b) Velocity vector over elliptical nose cone

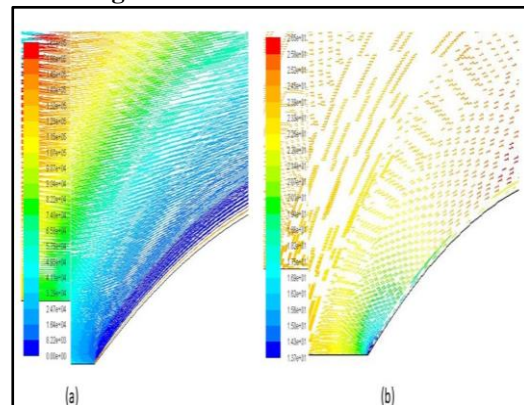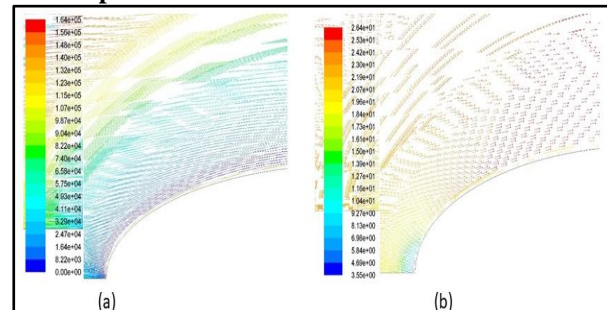# V. VARIATION OF COEFFICIENT OF DRAG BETWEEN INVISCID AND K-Ω SST MODEL

Figure 17 represents the variation between the values of coefficient of drag between the secant ogive and elliptical nose cone for both the inviscid and k-ω SST turbulence models. As illustrated in the graph it is clear that the values of Cd for both the nose cones in case of k-ω SST model is much more than the value of Cd at in viscid turbulence model. This is due to the induction of skin friction drag in case of k-ω SST turbulent model. From the graph we can further conclude at in both the cases the Cd experienced by elliptical profile is less than that of secant ogive hence, elliptical nose cone will have better aerodynamic efficiency then secant ogive under these conditions.
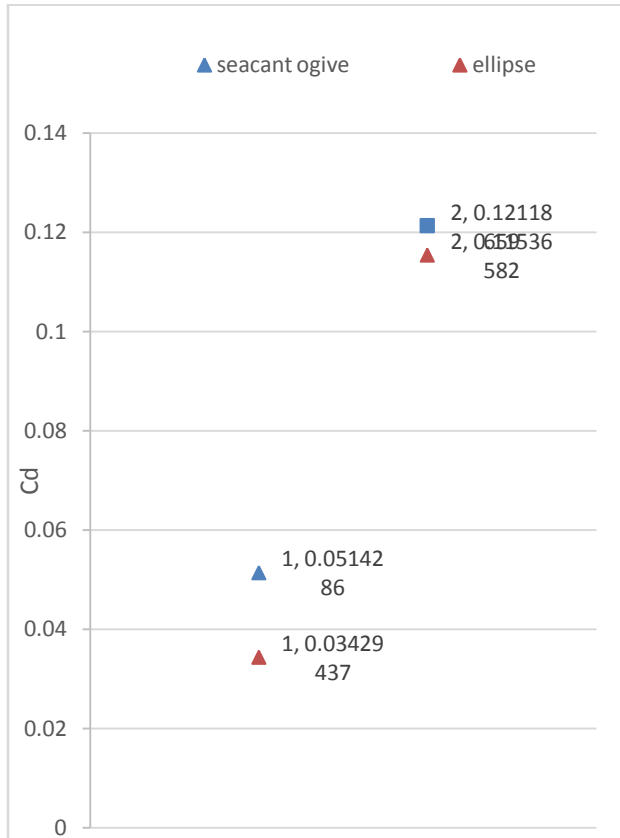

Figure 17Variation of coefficient of drag between inviscid and k-ω SST model.

VI.EXPERIMENTAL AND COMPUTATIONAL RESULT COMPARISON

The velocity, static pressure and coefficient of pressure were obtained experimentally and the results were plotted against the computational data obtained from the computational analysis in order to find out the deviation between them.

1. Comparison of Static Pressure For Secant Ogive And Elliptical Nose Cone

From the graph in the figure 18 we can conclude that the range of static pressure in case of ellipse ogive is much more than that of secant ogive. Furthermore, the nature of the curve for both the nose cones as seen is different. It is observed that the change in absolute pressure in case of ellipse is steeper when compared to that of secant ogive. This happen mainly due to the nature of shape of both the nose cones while secant ogive being more pointed towards its trailing edge doesn't create that much of stagnation whereas on the other hand the ellipse nose cone profile being more blunt creates a stagnation point much higher than that of the secant ogive.

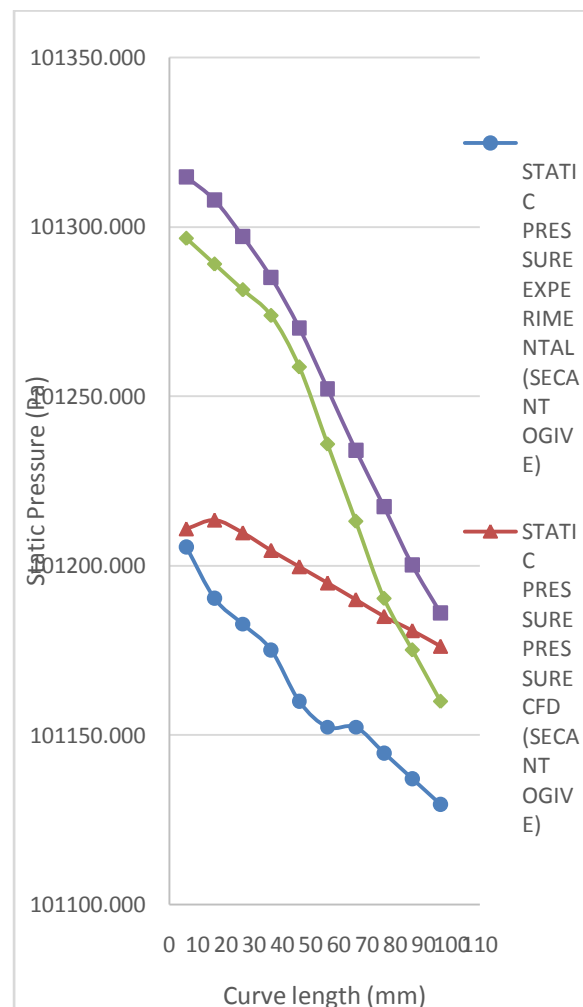Figure 18Static pressure comparison between secant ogive and elliptical nose cone

2. Comparison of Coefficient of Pressure for Secant Ogive And Elliptical Nose Cone

From the graph in figure 19 we can observe that the nature of curve for coefficient of pressure variation in

both secant ogive and elliptical nose cone is similar. The only difference between the two is that while the values of Cp start decreasing gradually in terms of secant ogive while the decrement in Cp in case of elliptical nose cone is steeper. The driving factor behind this type of behaviour is the bluntness of the leading edge of both the profiles. The stagnation created due to bluntness of the ellipse nose cones at the leading edge also leads to this steep decrease of value in Cp as compared to secant ogive. Since secant ogive is pointed at its leading edge the flow doesn't stagnate at the leading edge as much as it does in case of ellipse as a result of which the Cp values start decreasing gradually.
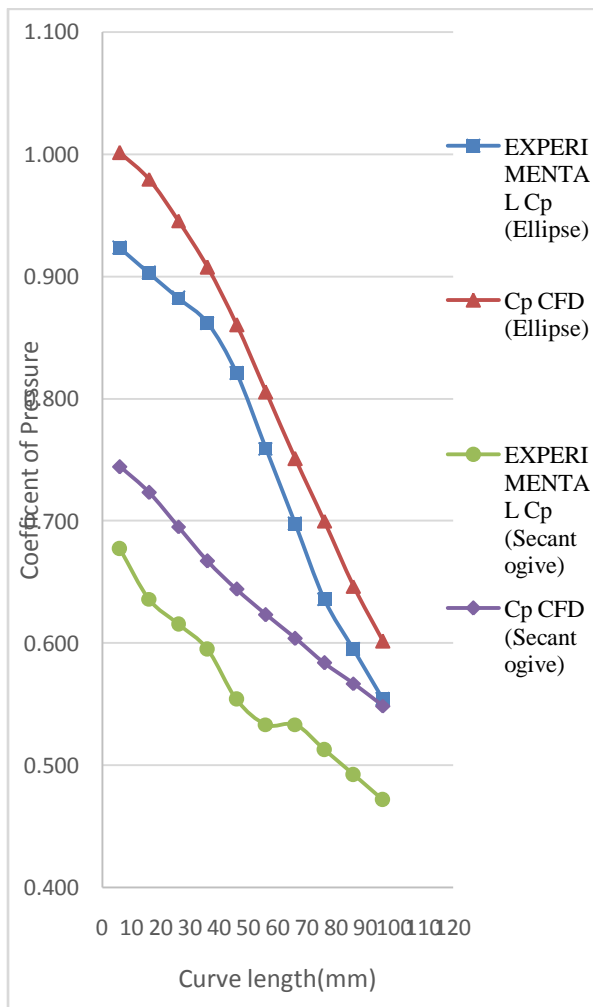
velocity at both the leading and the trailing edge is more in terms of secant ogive. In fact in case of secant ogive there is 64% increment in the velocity at the leading edge and 8.09% increment when compared to that of the ellipse profile. These profiles exhibit this kind of behaviour due to the formulation of stagnation point at the leading edge since the elliptical profile is blunter in comparison with the secant ogive. As a result it takes much longer for the fluid to accelerate over elliptical profile in comparison to secant ogive.

Figure 19 Coefficient of pressure comparison between secant ogive and elliptical nose cone
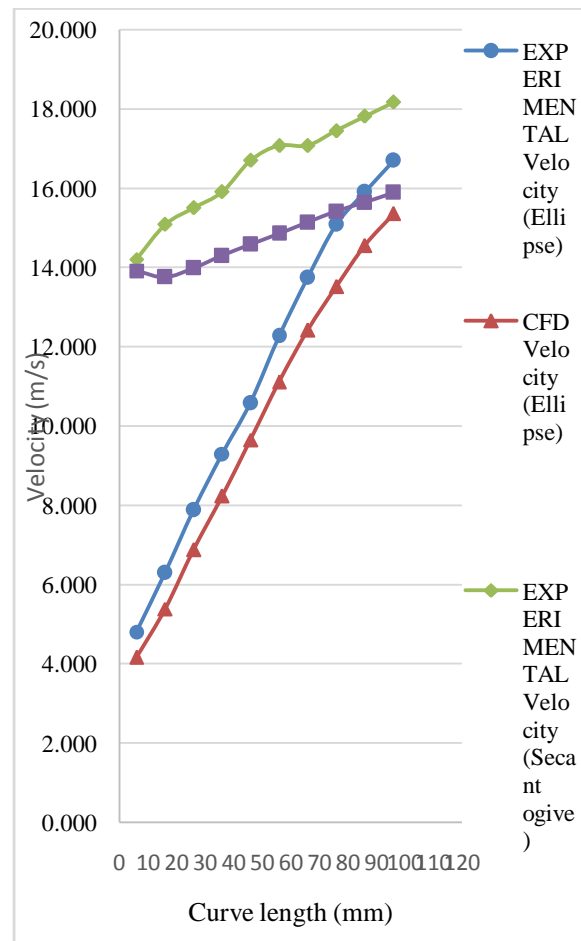
Figure 20 Velocity comparison between secant ogive and elliptical nose cone

3. Comparison of Velocity For Secant Ogive And Elliptical Nose Cone

The curvesin figure 20 compares both the CFD and the experimental values of the velocity over the curve length of both the profiles. It is observed from the curve that the

VII.OBSERVATIONS

After plotting and reviewing both the CFD and experimental data the following observations were made. In Table 4, 5 and 6 the deviation % between the experimental and numerical values for static pressure, coefficient of pressure and velocity has been represented for secant ogive. The same has been done in Tables 7, 8 and 9 for the elliptical nose cone.

Table 4 Deviation in Static pressure (Secant ogive)

	Distance from tip (mm)	Static pressure		Deviation %
		Experimental	Numerical	
P1	6	101205.535	101210.963	0.005
P2	16	101190.351	101213.550	0.023
P3	26	101182.759	101209.792	0.027
P4	36	101175.167	101204.598	0.029
P5	46	101159.983	101199.777	0.039
P6	56	101152.391	101194.986	0.042
P7	66	101152.391	101190.073	0.037
P8	76	101144.799	101185.104	0.040
P9	86	101137.207	101180.917	0.043
P10	96	101129.615	101176.295	0.046

Table 5 Deviation in Coefficient of pressure- (Secant ogive)

Points	Distance from tip (mm)	Cp		Deviation %
		Experimental	Numerical	
P1	6	0.677	0.744	9.030
P2	16	0.636	0.723	12.079
P3	26	0.616	0.695	11.463
P4	36	0.595	0.667	10.802
P5	46	0.554	0.644	13.993
P6	56	0.533	0.623	14.418
P7	66	0.533	0.604	11.670
P8	76	0.513	0.584	12.166
P9	86	0.492	0.567	13.142
P10	96	0.472	0.549	13.981

Table 6 Deviation in Velocity- (Secant ogive)

Points	Distance from tip (mm)	Velocity (m/s)		Deviation %
		Experimental	Numerical	
P1	6	14.206	13.915	2.044
P2	16	15.081	13.757	8.785
P3	26	15.501	13.987	9.768
P4	36	15.909	14.298	10.124
P5	46	16.696	14.582	12.661
P6	56	17.075	14.858	12.985
P7	66	17.075	15.136	11.356
P8	76	17.447	15.412	11.661
P9	86	17.811	15.641	12.179
P10	96	18.167	15.890	12.532

Table 7 Deviation in Absolute pressure- (Ellipse)

Points	Distance from tip (mm)	Static pressure		Deviation %
		Experimental	Numerical	
P1	12	101666.638	101695.468	0.028
P2	22	101659.046	101687.452	0.028
P3	32	101651.454	101674.845	0.023
P4	42	101643.862	101660.739	0.017
P5	52	101628.678	101643.382	0.014
P6	62	101605.902	101623.084	0.017
P7	72	101583.127	101602.833	0.019
P8	82	101560.351	101583.964	0.023
P9	92	101545.167	101564.230	0.019
P10	102	101529.983	101547.645	0.017

Table 8 Deviation in Coefficient of pressure- (Ellipse)

Points	Distance from tip (mm)	Cp		Deviation %
		Experimental	Numerical	
P1	12	0.923	1.001	7.784
P2	22	0.903	0.980	7.841
P3	32	0.882	0.946	6.690
P4	42	0.862	0.907	5.032
P5	52	0.821	0.861	4.624
P6	62	0.759	0.806	5.770
P7	72	0.698	0.751	7.100
P8	82	0.636	0.700	9.126
P9	92	0.595	0.647	7.976
P10	102	0.554	0.602	7.941

Table 9 Deviation in Velocity- (Ellipse)

Points	Distance from tip (mm)	Cp		Deviation %
		Experimental	Numerical	
P1	12	0.923	1.001	7.784
P2	22	0.903	0.980	7.841
P3	32	0.882	0.946	6.690
P4	42	0.862	0.907	5.032
P5	52	0.821	0.861	4.624
P6	62	0.759	0.806	5.770
P7	72	0.698	0.751	7.100
P8	82	0.636	0.700	9.126
P9	92	0.595	0.647	7.976
P10	102	0.554	0.602	7.941

The deviation in the following results is mainly due to human and mechanical error. The experimental analysis has been done on 3D profiles whereas the numerical analysis was carried out in 2D which might add to the deviation in the results.

VIII. CONCLUSION AND FUTURE SCOPE OF WORK

In this paper, the computational and experimental approach was used to study the aerodynamic performance of various nose cone such as pressure, coefficient of pressure, absolute pressure, axial velocity etc. of the various nose cone profiles were obtained for low subsonic conditions profiles for the same length to diameter ratio. The study involves an inlet velocity of 25 m/s that is calculated for zero angle of attack. The data obtained from the computational analysis of these nose cones profiles was then compared with experimental data obtained from wind tunnel analysis in order to find the deviation.

Coefficient of drag was the key parameter for the selection of the optimum shape for the subsonic flow range between secant ogive and elliptical nose cone profile. In the case of secant ogive nose cone the velocity was found to be 18.167 m/s near the trailing edge. The coefficient of pressure was found to be maximum at the tip of the nose cone while dynamic pressure was maximum at the trailing edge of the nose cone. The total drag experienced by secant ogive was 3.31 N corresponding to 0.12118659 value of Cd.In the case of elliptical nose cone the velocity was found to be 16.696 m/s near the trailing edge.

The coefficient of pressure was found to be maximum at the tip of the nose cone while dynamic pressure increased drastically as compared to secant ogive and was maximum at the trailing edge of the nose cone. The total drag experienced by secant ogive was 2.91 N corresponding to 0.11536583 value of Cd i.e. Coefficient of drag.Therefore we can conclude that on the basis of drag experienced by both the nose cones the elliptical nose cone experiences less drag when compared to that of Secant ogive hence elliptical ogive would perform better at these conditions when compared to the secant ogive.

These profiles can further be used in hypersonic and supersonic flow range and data such as velocity, dynamic pressure, static pressure and total drag over these profiles can be calculated in order to find the optimum profile in these flow ranges. There are also other profiles such as hemispherical, elliptical, power series, hack series that can be further tested for various aerodynamic parameters and optimum profile can be selected for different flow ranges or as per mission requirement.

REFRENCES

[1] J.D.Anderson, "Fundementals of Aerodynamics," in Fundementals of Aerodynamics, Fourth Edition, McGraw-Hill, 2007.

[2]Garry A. Crowell Sr., "The Descriptive Geometry of Nose Cone," 1996

[3]Bharti, Manish. (2016). Mathematical Modeling of Ogive Forebodies and Nose Cones. International Research Journal of Engineering and Technology. 3. 744.

[4]Dulikravich, "Three Dimensional Aerodynamic Shape Optimization Using Genetic and Gradient Search Algorithims," Journal of Rockets and Spacecrafts, Vol. 43, 1997.

[5]Lee, Jae-Woo & Byun, Yung-Hwan & Kim, Sang-Jin & Min, Byung-Young. (2006). Multipoint Nose Shape Optimization of Space Launcher Using Response Surface Method. Journal of Spacecraft and Rockets - J SPACECRAFT ROCKET. 43. 137-146. 10.2514/1.11228.

[6]R. J. Felkel, "Effect of Different Nose Profiles on Subsonic Pressure Coefficients," Department of Mechanical and Aerospace Engineering , California State University.

[7]Munk, "The Aerodynamic Forces on Airships Hulls," National Advisory Committee for Aeronautics, Report No. 184.

[8]Ashish Narayan, S Narayanan and Rakesh Kumar, Hypersonic flow past nose cones of different geometries: a comparative study

[9]H. S, D.Hasen and V.Giridharan, "CFD Study on Surface Pressure Distriibution and Base Pressure Distribution over Parabolic Series Nose Cone," Department of Aeronautical Engineering, Bharat Institute of Higher Education and Research.

[10]J. Sodja, "Turbulence Models in CFD," University of Ljubljana, 2007.

[11]L.Davidson, "An Introduction to Turbulence Models," Chalmers University of Technology, Getborg , Sweden, 2003.

[12]F.R.Menter, "Two Equation Eddy Viscosity Turbulence Models For Engineering Applications," 1994.